APL Materials

Band structure engineering of chemically tunable LnSbTe (Ln = La, Ce, Pr)

Cite as: APL Mater. **7**, 101113 (2019); https://doi.org/10.1063/1.5123396
Submitted: 05 August 2019 . Accepted: 15 September 2019 . Published Online: 15 October 2019

Ashley Weiland, David G. Chaparro, Maia G. Vergniory, Elena Derunova, Jiho Yoon, Iain W. H. Oswald, Gregory T. McCandless, Mazhar Ali, and Julia Y. Chan

Band structure engineering of chemically tunable LnSbTe (Ln = La, Ce, Pr)

Cite as: APL Mater. 7, 101113 (2019); doi: 10.1063/1.5123396
Submitted: 5 August 2019 • Accepted: 15 September 2019 •
Published Online: 15 October 2019

Ashley Weiland,[1] David G. Chaparro,[1] Maia G. Vergniory,[2] Elena Derunova,[3] Jiho Yoon,[3] Iain W. H. Oswald,[1] Gregory T. McCandless,[1] Mazhar Ali,[3,a)] and Julia Y. Chan[1,a)]

AFFILIATIONS

[1]Department of Chemistry and Biochemistry, The University of Texas at Dallas, Richardson, Texas 75080, USA
[2]Donostia International Physics Center, 20018 Donostia-San Sebastian, Spain and IKERBASQUE, Basque Foundation for Science, Maria Diaz de Haro 3, 48013 Bilbao, Spain
[3]Max Planck Institute of Microstructure Physics, Weinberg 2, 06120 Halle, Germany

Note: This paper is part of the Special Topic on Topological Semimetals—New Directions.
[a)]**Authors to whom correspondence should be addressed:** Maz@berkeley.edu and Julia.Chan@utdallas.edu

ABSTRACT

The ZrSiS family of compounds has garnered interest as Dirac nodal-line semimetals and offers an approach to study structural motifs coupled with electronic features, such as Dirac crossings. CeSbTe, of the ZrSiS/PbFCl structure type, is of interest due to its magnetically tunable topological states. The crystal structure consists of rare earth capped square nets separating the magnetic Ce–Te layers. In this work, we report the single crystal growth, magnetic properties, and electronic structures of $LnSb_{1-x}Bi_xTe$ (Ln = La, Ce, Pr; x ~ 0.2) and CeBiTe, adopting the CeSbTe crystal structure, and the implication of tuning the electronic properties by chemical substitution.

The discovery of fabricable and measurable topological materials has remained difficult over the last decade, despite a plethora of material predictions.[1–9] While many of the known topological phases are nonmagnetic (Cd_3As_2,[10,11] Na_3Bi,[12] and TaAs[4,5]), there is an increasing demand to find and investigate magnetic topological phases due to the added/broken symmetry effects of magnetic order parameters. One approach to finding novel topological phases is to look at materials with structural features which, by symmetry, demand electronic features—such as Dirac crossings—in the band structure. For example, nonmagnetic square nets are known to create Dirac nodal lines (DNL) due to the nonsymmorphic symmetry demanded band degeneracies.[13,14] A glide plane, in particular, protects the degeneracies from spin orbit coupling (SOC) opening a hybridization gap and preserves the DNL. In the case of time reversal symmetry (TRS) breaking magnetism, the DNL will split into Weyl nodal lines (WNL).[15,16]

From the perspective of structural features that would lead to symmetry-protected semimetals, one strategy is to consider crystal structures with square nets. Square nets are found as structural motifs in both the iron and cuprate superconductors.[17–20] In topological compounds, they were first featured in the layered magnetic phases $AMnBi_2$ (A = Yb, Sr, and Eu), which consist of layers of Bi square nets, magnetic layers with Mn–Bi, and A-site cations such as Yb^{2+}, Sr^{2+}, and Eu^{2+}.[21,22] More recently, the layered, nonmagnetic ZrSiX (X = S, Se, and Te)[6,23–26] phases were found to be topologically tunable through manipulation of the X site. In particular, the nonsymmorphic symmetry demands a degeneracy at the X point in the first Brillouin zone and preserves that degeneracy along the X-M line. A structural analog of the ZrSiX phases is CeSbTe, which has Sb square nets interleaved with Ce–Te layers. In this compound, the Ce^{3+} results in a spin ½ system and low temperature magnetic ordering with B-field dependent metamagnetic transitions, resulting in both time reversal symmetry (TRS) breaking and non-TRS breaking states.[27] TRS-breaking topological phases are another popular avenue of research due to the possibility for studying the interplay between magnetism and topology as well as the Berry curvature and topological character which can give rise to exotic physical phenomena such as the anomalous and quantum anomalous hall effects seen

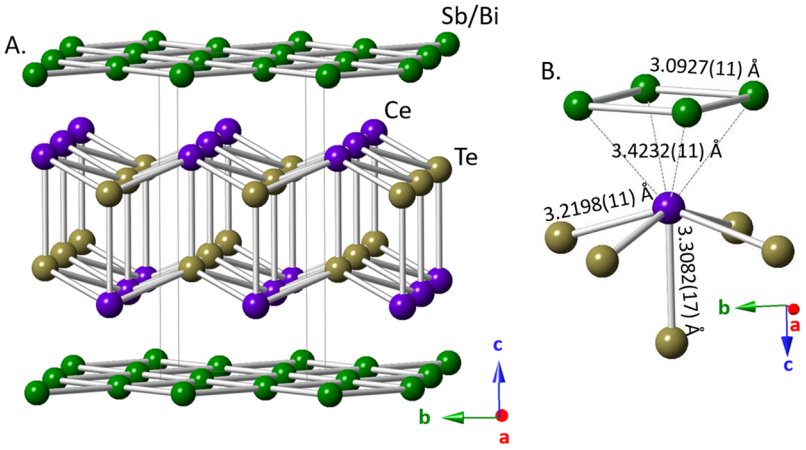

FIG. 1. The layered structure of $CeSb_{1-x}Bi_xTe$ (a) and the coordination of Ce by four Sb/Bi and five Te with various bonding distances highlighted (b). Rare earth elements are represented by purple, tellurium in tan, and antimony/bismuth in green. A small amount of Bi is incorporated into the Sb square net site.

in $Co_3Sn_2S_2$ and Cr-doped Bi_2Te_3.[28,29] Hence, CeSbTe is an interesting system to study since it is tunable topologically between hosting Weyl and Dirac carriers but suffers from a large topologically trivial pocket near the Fermi level at Γ in the electronic structure.[27] This results in a large fraction of the Fermi sea comprising topologically trivial electrons, making topological transport properties difficult to discern. Ideally, through chemical control, the electronic structure of this material could be engineered to gap out the trivial pocket while preserving the magnetism and the topologically relevant features.

Here, we report the single crystal growth, magnetic properties, and electronic structures of $LnSb_{1-x}Bi_xTe$ (Ln = La, Ce, Pr; x ~ 0.2) and CeBiTe, isostructural to CeSbTe. We show that by controlling the chemical composition (by modifying both the rare-earth element as well as the square net element), the unit cell size can be tuned without changing the symmetry and the band structure is engineered toward the topologically ideal case. Specifically, we find that CeBiTe, with a larger square net, has dramatically reduced the size of the trivial pocket while keeping the Dirac crossing at X near the Fermi level. In addition, a heavily doped $LaSb_{1-x}Bi_xTe$, as close to LaBiTe as possible, is expected to completely gap the trivial pocket and be an ideal nonsymmorphic topological semimetal. Magnetically, $CeSb_{1-x}Bi_xTe$ and CeBiTe show metamagnetic transitions and have ordering temperatures similar to that of CeSbTe.

Single crystals of $LnSb_{1-x}Bi_xTe$ (Ln = La, Ce, Pr; x ~ 0.2) were grown using an elemental ratio of 1.2:1:1:12 of Ln (La, Ce, and Pr), Sb, Te, and Bi, respectively, and 1.2:1:13 for CeBiTe. Ln, Sb, and Te were sandwiched between Bi shots in an alumina crucible, which was capped with a sieve and a catch alumina crucible, also known as a Canfield crucible set.[30] The bismuth flux was utilized to allow a eutectic mixture to form. The crucibles were placed in a 14 mm outer diameter fused-silica tube, sealed under ~1/3 atm Ar, and placed in a programmable furnace. The heating profile began at 300 °C and increased to 1100 °C at a rate of 50 °C/h. The temperature was held at 1100 °C for a total of 120 h, until it slowly cooled to 675 °C at a rate of 5 °C/h. The reaction vessels were removed from the furnace and centrifuged for ~5 min to separate the extra bismuth from the

TABLE I. Crystallographic parameters of $LnSb_{1-x}Bi_xTe$ (Ln = La, Ce, Pr; x ~ 0.2) and CeBiTe.

P4/nmm	$LaSb_{0.770(6)}Bi_{0.230(6)}Te$	$CeSb_{0.836(4)}Bi_{0.164(4)}Te$	$PrSb_{0.864(7)}Bi_{0.136(7)}Te$	CeBiTe
a (Å)	4.4115(15)	4.3737(15)	4.3532(2)	4.4594(1)
c (Å)	9.578(4)	9.471(4)	9.4180(5)	9.4722(3)
V (Å^3)	186.39(15)	181.17(15)	178.47(2)	188.37(1)
Temperature (K)	298	298	298	298
θ range (deg)	5.1–30.4	5.1–30.5	4.3–30.5	4.3–30.4
μ (mm^{-1})	35.12	34.24	34.40	65.89
Measured reflns	1666	1672	2606	1955
Independent reflns	207	200	197	208
R_{int}	0.035	0.034	0.031	0.066
$\Delta\rho_{max}$ (e Å^{-3})	0.86	0.89	0.96	5.86
$\Delta\rho_{min}$ (e Å^{-3})	−1.49	−2.56	−2.38	−3.69
Extinction coeff	0.0385(18)	0.0300(13)	0.0263(16)	0.044(4)
R_1 [$F^2 > 2\sigma(F^2)$]	0.016	0.016	0.017	0.037
wR_2 (F^2)	0.035	0.032	0.038	0.097

TABLE II. Atomic positions of $LnSb_{1-x}Bi_xTe$ (Ln = La, Ce, Pr; x ~ 0.2) and CeBiTe.

Site label	Wyckoff	x	y	z	U_{eq}	Occupancy
			$LaSb_{0.780(5)}Bi_{0.220(5)}Te$			
La	2*c*	$\frac{1}{4}$	$\frac{1}{4}$	0.279 11(5)	0.007 64(17)	1
Sb	2*a*	$\frac{3}{4}$	$\frac{1}{4}$	0	0.011 7(2)	0.780(5)
Bi	2*a*	$\frac{3}{4}$	$\frac{1}{4}$	0	0.011 7(2)	0.220(5)
Te	2*c*	$\frac{1}{4}$	$\frac{1}{4}$	0.627 47(5)	0.007 94(18)	1
			$CeSb_{0.836(4)}Bi_{0.164(4)}Te$			
Ce	2*c*	$\frac{1}{4}$	$\frac{1}{4}$	0.278 07(5)	0.006 95(15)	1
Sb	2*a*	$\frac{3}{4}$	$\frac{1}{4}$	0	0.009 46(19)	0.836(4)
Bi	2*a*	$\frac{3}{4}$	$\frac{1}{4}$	0	0.009 46(19)	0.164(4)
Te	2*c*	$\frac{1}{4}$	$\frac{1}{4}$	0.627 36(5)	0.007 08(16)	1
			$PrSb_{0.864(7)}Bi_{0.136(7)}Te$			
Pr	2*c*	$\frac{1}{4}$	$\frac{1}{4}$	0.277 76(5)	0.008 17(17)	1
Sb	2*a*	$\frac{3}{4}$	$\frac{1}{4}$	0	0.010 9(2)	0.856(5)
Bi	2*a*	$\frac{3}{4}$	$\frac{1}{4}$	0	0.010 9(2)	0.144(5)
Te	2*c*	$\frac{1}{4}$	$\frac{1}{4}$	0.627 15(6)	0.008 26(18)	1
			CeBiTe			
Ce	2*c*	$\frac{1}{4}$	$\frac{1}{4}$	0.283 83(10)	0.003 0(4)	1
Bi	2*a*	$\frac{3}{4}$	$\frac{1}{4}$	0	0.004 6(4)	1
Te	2*c*	$\frac{1}{4}$	$\frac{1}{4}$	0.630 25(12)	0.003 8(4)	1

reaction mixture, resulting in single crystals ~0.5–0.8 mm in size with a tablet morphology.

Single crystals were mounted on glass fibers using a two-part epoxy. Data were collected with a Bruker D8 Quest Kappa single-crystal X-ray diffractometer with a Mo Kα source (λ = 0.710 73), a HELIOS optics monochromator, and a Photon 100 CMOS detector. The collected data were corrected for absorption using the multiscan method with Bruker program SADABS. Starting crystallographic models were obtained using the intrinsic phasing method in SHELXT[31] and then refined using SHELXL2014.[32]

First principles calculations were performed using Density Functional Theory (DFT) as implemented in the Vienna *ab initio* Simulation Package (VASP).[33–36] The interaction between ion cores and valence electrons was treated by the projector augmented-wave method, the generalized gradient approximation (GGA) for the exchange-correlation potential with Perdew-Burke-Ernkzerhof for solids parametrization,[37] and spin-orbit coupling was taken into account by the second variation method.[38] F-electrons were included in the core as recommended by Ref. 39. A Gamma-centered k-point grid of (11 × 11 × 11) for reciprocal space

TABLE III. Select bond distances of $LnSb_{1-x}Bi_xTe$ (Ln = La, Ce, Pr; x ~ 0.2) and CeBiTe.

	CeSbTe	$CeSb_{1-x}Bi_xTe$	CeBiTe	$PrSb_{1-x}Bi_xTe$	$LaSb_{1-x}Bi_xTe$
Ln–Pn (Å)	3.3939	3.423 2(11)	3.492 8(7)	3.403 1(4)	3.465 7(10)
Pn–Pn (Å)	3.1176	3.092 7(11)	3.153 3(1)	3.078 2(1)	3.119 4(11)

integration and 550 eV energy cutoff of the plane-wave expansion have been used to get a residual error on the energy of less than 10^{-3} meV, resulting in a fully converged electronic structure including spin-orbit coupling. All the electronic structures are calculated based on experimental lattice constants, including spin orbit coupling (SOC).

Temperature dependent magnetic susceptibility measurements were performed using a Quantum Design MPMS3 SQUID magnetometer in VSM mode up to 7 T. The field dependence of magnetization curves at 2 K was obtained with a uniform field sweeping range from −7 T to 7 T. See the supplementary material for temperature and field dependent magnetic susceptibility.

$LnSb_{1-x}Bi_xTe$ (Ln = La, Ce, Pr; x ~ 0.2) and CeBiTe crystallize in a well-known structure type, ZrSiS (also known as PbFCl).[40] This structure type is best modeled in the tetragonal *P4/nmm* space group (No. 129) with Ln, Sb/Bi, and Te, occupying the 2*c*, 2*a*, and 2*c* sites, respectively. The lanthanide caps five Te atoms forming a distorted square pyramid, and antimony square nets are separated from the Ce–Te slab by van der Waals forces, as shown in Fig. 1. In $LnSb_{1-x}Bi_xTe$ (Ln = La, Ce, Pr; x ~ 0.2), an excess of electron density on the Sb site indicates a small amount of a heavier element also present on the Sb site; therefore, this site was modeled as a mixed site with both Sb and Bi, as described elsewhere.[41] The lack of additional electron density on the Te site indicates that Bi is not present on the Te site. Bi can indeed be incorporated into the Sb square nets as evident in $Ce_2Fe_{4-x}Co_xSb_5$.[42] In the title compounds, we determined the compositions as $LnSb_{1-x}Bi_xTe$, where x ~ 0.22, 0.16, and 0.14 for Ln = La, Ce, and Pr, respectively.

Crystallographic information can be found in Table I, positional details in Table II, and relevant bond distances in Table III. Figure 2 shows the lattice parameters of CeSbTe, $LnSb_{1-x}Bi_xTe$ (Ln = La, Ce, Pr; x ~ 0.2), and CeBiTe, demonstrating the tunability of the unit cell dimensions. Figure S1 shows the temperature dependent magnetic susceptibility of $CeSb_{1-x}Bi_xTe$ and CeBiTe. $CeSb_{1-x}Bi_xTe$ orders antiferromagnetically at T_N = 2.55 K, where μ_{eff} = 2.58 μ_B and CeBiTe orders at ~2 K with μ_{eff} = 2.00 μ_B. There is no significant change as compared to the CeSbTe which orders at T_N ~ 2 K at 0.5 T and μ_{eff} = 2.50 μ_B. Figure S2 shows the magnetization as a function of field for $CeSb_{1-x}Bi_xTe$ and CeBiTe. CeSbTe, $CeSb_{1-x}Bi_xTe$, and CeBiTe have similar metamagnetic transitions at 0.2 T, 0.9 T, and 0.15 T, respectively, similar to the "Devil's Staircase" material, CeSbSe, where stepwise transitions are present between 1.3 and 1.9 T.[43] Figure S3 shows the temperature dependent magnetic susceptibility and the magnetization as a function of field for $PrSb_{1-x}Bi_xTe$, which is a paramagnet with a u_{eff} = 3.51 μ_B comparable to the u_{calc} of a free Pr^{3+} ion of 3.58 μ_B.

The electronic structure of the parent compound, CeSbTe, in the nonmagnetic state is shown in Fig. 3(a); the nonsymmorphic symmetry demanded crossing at X lies just below the Fermi level and the two bands fold together along the X-M line. A large topologically trivial pocket is present at Γ.[27] Substitution of 10% Bi into the square nets of CeSbTe ($CeSb_{1-x}Bi_xTe$) surprisingly shrinks the Sb/Bi square net despite the larger covalent radii. Further investigations into the possibility of a minute structural distortion below the resolution limit of our single crystal X-ray diffractometer will be carried out in the future. However, in the current model, the modification of the unit cell due to partial Bi incorporation leads to a decrease in the trivial pocket at Γ (valence band maximum decreased from ~0.29 eV to ~0.2 eV); however, the bands still touch, as shown in Fig. 3(b). The nonsymmorphic degeneracy at X also raised from −0.1 eV below the Fermi level to being almost exactly at the Fermi level. Completely replacing Sb with Bi in the crystal structure (CeBiTe) leads to a widening along the *a*-direction and an increased square net size (see Table III) as well as an increase in the distance between the Sb square net and the Ln layer (longer *c*-axis). This corresponded to a further decrease in the size of the trivial pocket. Another sharper pocket sets the new valence band maximum at ~0.1 eV. $LaSb_{1-x}Bi_xTe$ has a similar *a*-lattice dimension to CeSbTe, but a much larger *c*-lattice parameter, and as can be seen in Fig. 3(e), the trivial bands are pulled apart and the rest of the structure is left unchanged. The increased spacing between the square net and the Ln layer caused a gap to open, likely making $LaSb_{1-x}Bi_xTe$ a weak TI, similar to LaSbTe.[44] However, both of these phases suffer again from the large trivial

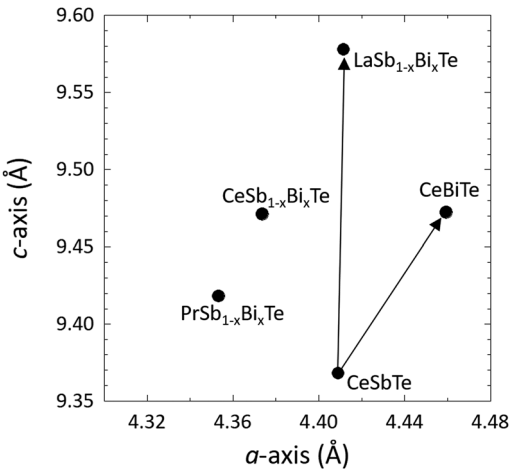

FIG. 2. The unit cell dimensions of CeSbTe, $LnSb_{1-x}Bi_xTe$ (Ln = La, Ce, Pr; x ~ 0.2), and CeBiTe. Incorporating Bi into the Sb square net site of CeSbTe increases the unit cell in the *c*-direction, while completely replacing Sb with Bi increases the unit cell in both the *c*- and *a*-directions. Replacing the rare earth site in $CeSb_{1-x}Bi_xTe$ with Pr decreases the unit cell in both the *c*- and *a*-directions while replacing with La increases both the *c*- and *a*-directions.

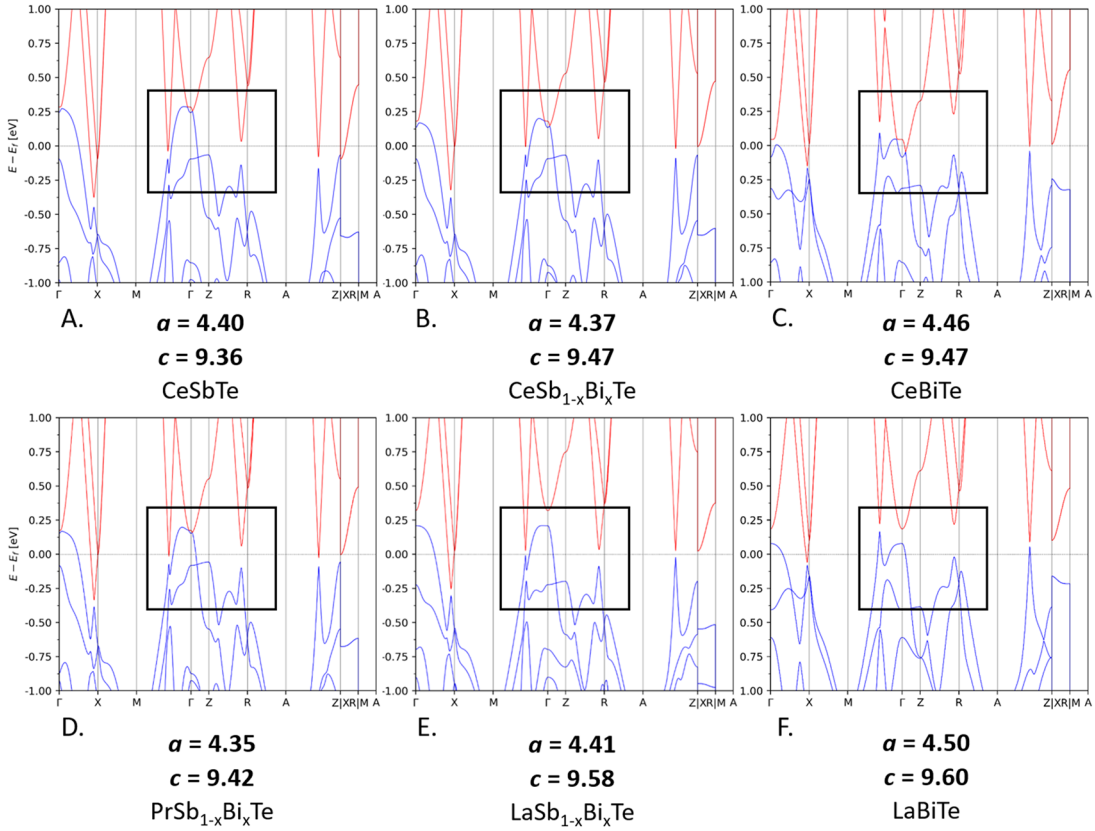

FIG. 3. Band structure calculations of (a) $CeSbTe$, (b) $CeSb_{1-x}Bi_xTe$, (c) $CeBiTe$, (d) $PrSb_{1-x}Bi_xTe$, (e) $LaSb_{1-x}Bi_xTe$, and theoretical compound $LaBiTe$ (f). $CeSbTe$ and $LaSb_{1-x}Bi_xTe$ have similar *a*-axis dimensions, demonstrating how the band structure changes as the *c*-axis is increased. $PrSb_{1-x}Bi_xTe$, $CeSb_{1-x}Bi_xTe$, and $CeBiTe$ have similar *c*-axis dimensions, demonstrating how the band structure changes as the square net bond distances are modified.

pocket which would result in trivial bulk conduction, dominating the transport properties over the Dirac carriers (either from the surface state or from the Dirac degeneracy at X). However, combining the result of the Bi substitution into the square net layer with the result of La substitution for Ce in the Ln layer, we proposed that a larger unit cell (a ~ 4.5, c ~ 9.6 Å) would result in an ideal band structure, where the trivial pocket at Γ will be gapped and its contribution to the Fermi surface minimal. A more heavily Bi-doped $LaSb_{1-x}Bi_x$ or a hypothetical $LaBiTe$ phase could realize this [Fig. 3(f)].

Here, we have shown that with the incorporation of Bi and substitution of the rare earth element, the crystallographic dimensions were able to be tuned without altering the symmetry of the system, thereby tuning the band dispersions without significantly changing the habit of the electronic structure. There is a precedence of Bi substitution in Sb square nets; in $Ce_2Fe_{4-x}Co_xSb_5$, Bi was incorporated in square net environments without significantly impacting the crystallographic structure or magnetic properties.[42] There are also a variety of other dopants (Ln = magnetic rare earth) which could be substituted in conjunction with Sb/Bi mixing to modify the band structure. The $LnSb_{1-x}Bi_xTe$ chemical family allows for a variety of topological/trivial states to be controlled both through magnetic order and band dispersion engineering.

Please see the supplementary material for magnetic data. X-ray crystallographic information files (CIFs) for all compounds are available free of charge via the Internet at www.ccdc.cam.ac.uk/data_request/cif. The associated deposition numbers for $LaSb_{1-x}Bi_xTe$, $CeSb_{1-x}Bi_xTe_x$, $CeBiTe$, and $PrSb_{1-x}Bi_xTe$ are 1 882 880, 1 882 879, 1 882 882, and 1 882 881, respectively.

The authors acknowledge Grant No. NSF-DMR-1700030 for partial funding of this work. M.G.V. was supported by Grant No. IS2016-75862-P national project of the Spanish MINECO. M.A., E.D., and J.Y. acknowledge the Alexander von Humboldt Foundation and their Sofja Kovalevskaja Award as well as the German Federal Ministry of Education and Research and the Minerva Foundation.

The authors declare no competing financial interest.

REFERENCES

[1] C. L. Kane and E. J. Mele, Science **314**, 1692 (2006).
[2] L. Fu and C. L. Kane, Phys. Rev. B **76**, 045302 (2007).
[3] D. Hsieh, D. Qian, L. Wray, Y. Xia, Y. S. Hor, R. J. Cava, and M. Z. Hasan, Nature **452**, 970 (2008).
[4] L. X. Yang, Z. K. Liu, Y. Sun, H. Peng, H. F. Yang, T. Zhang, B. Zhou, Y. Zhang, Y. F. Guo, M. Rahn, D. Prabhakaran, Z. Hussain, S. K. Mo, C. Felser, B. Yan, and Y. L. Chen, Nat. Phys. **11**, 728 (2015).

[5]S.-Y. Xu, I. Belopolski, N. Alidoust, M. Neupane, G. Bian, C. Zhang, R. Sankar, G. Chang, Z. Yuan, C.-C. Lee, S.-M. Huang, H. Zheng, J. Ma, D. S. Sanchez, B. Wang, A. Bansil, F. Chou, P. P. Shibayev, H. Lin, S. Jia, and M. Z. Hasan, Science **349**, 613 (2015).
[6]M. M. Hosen, K. Dimitri, I. Belopolski, P. Maldonado, R. Sankar, N. Dhakal, G. Dhakal, T. Cole, P. M. Oppeneer, D. Kaczorowski, F. Chou, M. Z. Hasan, T. Durakiewicz, and M. Neupane, Phys. Rev. B **95**, 161101 (2017).
[7]T. Zhang, Y. Jiang, Z. Song, H. Huang, Y. He, Z. Fang, H. Weng, and C. Fang, Nature **566**, 475 (2019).
[8]M. G. Vergniory, L. Elcoro, C. Felser, N. Regnault, B. A. Bernevig, and Z. Wang, Nature **566**, 480 (2019).
[9]F. Tang, H. C. Po, A. Vishwanath, and X. Wan, Nature **566**, 486 (2019).
[10]M. Neupane, S.-Y. Xu, R. Sankar, N. Alidoust, G. Bian, C. Liu, I. Belopolski, T.-R. Chang, H.-T. Jeng, H. Lin, A. Bansil, F. Chou, and M. Z. Hasan, Nat. Commun. **5**, 3786 (2014).
[11]Z. K. Liu, J. Jiang, B. Zhou, Z. J. Wang, Y. Zhang, H. M. Weng, D. Prabhakaran, S. K. Mo, H. Peng, P. Dudin, T. Kim, M. Hoesch, Z. Fang, X. Dai, Z. X. Shen, D. L. Feng, Z. Hussain, and Y. L. Chen, Nat. Mater. **13**, 677 (2014).
[12]Z. K. Liu, B. Zhou, Y. Zhang, Z. J. Wang, H. M. Weng, D. Prabhakaran, S.-K. Mo, Z. X. Shen, Z. Fang, X. Dai, Z. Hussain, and Y. L. Chen, Science **343**, 864 (2014).
[13]S.-Y. Yang, H. Yang, E. Derunova, S. S. P. Parkin, B. Yan, and M. N. Ali, Adv. Phys.: X **3**, 1414631 (2018).
[14]W. Tremel and R. Hoffmann, J. Am. Chem. Soc. **109**, 124 (1987).
[15]S. M. Young and C. L. Kane, Phys. Rev. Lett. **115**, 126803 (2015).
[16]S. Klemenz, S. Lei, and L. M. Schoop, Annu. Rev. Mater. Res. **49**(1), 185–206 (2019).
[17]C. C. Tsuei and J. R. Kirtley, Rev. Mod. Phys. **72**, 969 (2000).
[18]J. Paglione and R. L. Greene, Nat. Phys. **6**, 645 (2010).
[19]G. R. Stewart, Rev. Mod. Phys. **83**, 1589 (2011).
[20]D. N. Basov and A. V. Chubukov, Nat. Phys. **7**, 272 (2011).
[21]H. Masuda, H. Sakai, M. Tokunaga, A. Miyake, Y. Yamasaki, J. Shiogai, S. Nakamura, S. Awaji, A. Tsukazaki, H. Nakao, Y. Murakami, T.-H. Arima, Y. Tokura, and S. Ishiwata, Sci. Adv. **2**, e1501117 (2016).
[22]S. Borisenko, D. Evtushinsky, Q. Gibson, A. Yaresko, T. Kim, M. N. Ali, B. Buechner, M. Hoesch, and R. J. Cava, "Time-Reversal Symmetry Breaking Type-II Weyl State in YbMnBi2," e-print arXiv:1507.04847.
[23]M. Neupane, I. Belopolski, M. M. Hosen, D. S. Sanchez, R. Sankar, M. Szlawska, S.-Y. Xu, K. Dimitri, N. Dhakal, P. Maldonado, P. M. Oppeneer, D. Kaczorowski, F. Chou, M. Z. Hasan, and T. Durakiewicz, Phys. Rev. B **93**, 201104 (2016).
[24]J. Hu, Z. Tang, J. Liu, X. Liu, Y. Zhu, D. Graf, K. Myhro, S. Tran, C. N. Lau, J. Wei, and Z. Mao, Phys. Rev. Lett. **117**, 016602 (2016).
[25]M. N. Ali, L. M. Schoop, C. Garg, J. M. Lippmann, E. Lara, B. Lotsch, and S. S. P. Parkin, Sci. Adv. **2**(12), e1601742 (2016).
[26]L. M. Schoop, M. N. Ali, C. Straßer, A. Topp, A. Varykhalov, D. Marchenko, V. Duppel, S. S. P. Parkin, B. V. Lotsch, and C. R. Ast, Nat. Commun. **7**, 11696 (2016).
[27]L. M. Schoop, A. Topp, J. Lippmann, F. Orlandi, L. Müchler, M. G. Vergniory, Y. Sun, A. W. Rost, V. Duppel, M. Krivenkov, S. Sheoran, P. Manuel, A. Varykhalov, B. Yan, R. K. Kremer, C. R. Ast, and B. V. Lotsch, Sci. Adv. **4**(2), eaar2317 (2018).
[28]C.-Z. Chang, J. Zhang, X. Feng, J. Shen, Z. Zhang, M. Guo, K. Li, Y. Ou, P. Wei, L.-L. Wang, Z.-Q. Ji, Y. Feng, S. Ji, X. Chen, J. Jia, X. Dai, Z. Fang, S.-C. Zhang, K. He, Y. Wang, L. Lu, X.-C. Ma, and Q.-K. Xue, Science **340**, 167 (2013).
[29]E. Liu, Y. Sun, N. Kumar, L. Muechler, A. Sun, L. Jiao, S.-Y. Yang, D. Liu, A. Liang, Q. Xu, J. Kroder, V. Süß, H. Borrmann, C. Shekhar, Z. Wang, C. Xi, W. Wang, W. Schnelle, S. Wirth, Y. Chen, S. T. B. Goennenwein, and C. Felser, Nat. Phys. **14**, 1125 (2018).
[30]P. C. Canfield, T. Kong, U. S. Kaluarachchi, and N. H. Jo, Philos. Mag. **96**, 84 (2016).
[31]G. M. Sheldrick, Acta Crystallogr., Sect. A: Found. Adv. **71**, s273 (2015).
[32]G. M. Sheldrick, Acta Crystallogr., Sect. C: Struct. Chem. **71**, 3 (2015).
[33]G. Kresse and J. Hafner, Phys. Rev. B **47**, 558 (1993).
[34]G. Kresse and J. Hafner, Phys. Rev. B **49**, 14251 (1994).
[35]G. Kresse and J. Furthmüller, Comput. Mater. Sci. **6**, 15 (1996).
[36]G. Kresse and J. Furthmüller, Phys. Rev. B **54**, 11169 (1996).
[37]J. P. Perdew, K. Burke, and M. Ernzerhof, Phys. Rev. Lett. **77**, 3865 (1996).
[38]D. Hobbs, G. Kresse, and J. Hafner, Phys. Rev. B **62**, 11556 (2000).
[39]A. Jain, G. Hautier, C. J. Moore, S. Ping Ong, C. C. Fischer, T. Mueller, K. A. Persson, and G. Ceder, Comput. Mater. Sci. **50**, 2295 (2011).
[40]W. Nieuwenkamp and J. M. Bijvoet, Z. Kristallogr. - Cryst. Mater. **81**, 469 (1932).
[41]I. W. H. Oswald, Ph.D. dissertation (The University of Texas at Dallas, 2017), https://utd-ir.tdl.org/handle/10735.1/5963.
[42]A. Weiland, S. Li, K. A. Benavides, J. V. Burnett, J. Milam-Guerrero, A. J. Neer, G. T. McCandless, B. Lv, and J. Y. Chan, Inorg. Chem. **58**, 6028 (2019).
[43]K. W. Chen, Y. Lai, Y. C. Chiu, S. Steven, T. Besara, D. Graf, T. Siegrist, T. E. Albrecht-Schmitt, L. Balicas, and R. E. Baumbach, Phys. Rev. B **96**, 014421 (2017).
[44]R. Singha, A. Pariari, B. Satpati, and P. Mandal, Phys. Rev. B **96**, 245138 (2017).